Modification of a buried interface with bulky organic cations for highly stable flexible perovskite solar cells

Journal:	*ACS Applied Energy Materials*
Manuscript ID	ae-2022-02780r.R1
Manuscript Type:	Article
Date Submitted by the Author:	n/a
Complete List of Authors:	Dasgupta, Shyantan; Saule Research Institute; Poznan University of Technology Zuraw, Wiktor; Saule Research Institute; Wroclaw University of Science and Technology, Department of Semiconductor Materials Engineering Ahmad, Taimoor; Saule Technologies, Castriotta, Luigi Angelo; University of Rome Tor Vergata, CHOSE Radicchi, Eros; Universita degli Studi di Perugia; CNR, CNR-SCITEC, Dipartimento di Chimica, Universita' di Perugia MROZ, WOJCIECH; Consiglio Nazionale delle Ricerche, Istituto di Scienze e Tecnologie Chimiche "Giulio Natta" (SCITEC) Ścigaj, Mateusz; Saule Technologies Pawlaczyk, Łukasz; Wroclaw University of Science and Technology, Department of Nanometrology Tamulewicz-Szwajkowska, Magdalena; Wrocław University of Science and Technology, Department of Nanometrology Trzciński, Marek; UTP University of Science and Technology Serafińczuk, Jarosław; Wroclaw University of Science and Technology, Department of Nanometrology Mosconi, Edoardo; CNR, CNR-SCITEC, Dipartimento di Chimica, Universita' di Perugia Di Carlo, Aldo; University of Rome "Tor Vergata", CHOSE, Centre for Hybrid and Organic Solar Energy, Department Electronics Engineering De Angelis, Filippo; Universita degli Studi di Perugia Dipartimento di Chimica Biologia e Biotecnologie, Department of Chemistry, Biology and Biotechnology ; Universita degli Studi di Perugia Dipartimento di Chimica Biologia e Biotecnologie, Department of Chemistry, Biology and Biotechnology; CNR, CNR-SCITEC, Dipartimento di Chimica, Universita' di Perugia Dudkowiak, Alina; Politechnika Poznanska, Institute of Physics Wojciechowski, Konrad; Saule Research Institute; Saule Technologies

Modification of a buried interface with bulky organic cations for highly stable flexible perovskite solar cells

*Shyantan Dasgupta[a,b], Wiktor Żuraw[a,c], Taimoor Ahmad[d], Luigi Angelo Castriotta[e], Eros Radicchi[f,g], Wojciech Mróz[h,i], Mateusz Scigaj[d], Łukasz Pawlaczyk[j], Magdalena Tamulewicz-Szwajkowska[j], Marek Trzcinski[k], Jarosław Serafińczuk[j,l], Edoardo Mosconi[f], Aldo Di Carlo[e,m], Filippo De Angelis[f, n ,o], Alina Dudkowiak[b], Konrad Wojciechowski[a, d]**

*Corresponding author

[a] Saule Research Institute, Dunska 11, 54-427 Wroclaw, Poland
[b] Faculty of Materials Engineering and Technical Physics, Poznan University of Technology, Piotrowo 3, 60-965 Poznan, Poland
[c] Department of Semiconductor Materials Engineering, Wroclaw University of Science and Technology, Wybrzeze Wyspianskiego 27, 50-370, Wroclaw, Poland
[d] Saule Technologies, Dunska 11, 54-427 Wroclaw, Poland
[e] Centre for Hybrid and Organic Solar Energy (CHOSE), Department of Electronic Engineering, University of Rome Tor Vergata, Rome, 00133, Italy
[f] Computational Laboratory for Hybrid/Organic Photovoltaics (CLHYO), Istituto CNR di Scienze e Tecnologie Chimiche "Giulio Natta" (CNR-SCITEC), via Elce di Sotto 8, Perugia (PG), I-06123 Italy.
[g] Nanomaterials Research Group, Department of Biotechnology, University of Verona, Strada Le Grazie 15, I-37134 Verona, Italy.
[h] Centre for Nano Science and Technology (CNST@PoliMi), Istituto Italiano di Tecnologia (IIT), Via Pascoli, 70/3, 20133, Milano, Italy
[i] Istituto di Scienze e Tecnologie Chimiche "Giulio Natta" (SCITEC),Consiglio Nazionale delle Ricerche, v. A. Corti 12, 20133 Milan, Italy
[j] Department of Nanometrology, Wroclaw University of Science and Technology, Janiszewskiego 11/17, 50-372 Wroclaw, Poland
[k] Institute of Mathematics and Physics, Bydgoszcz University of Science and Technology; Al. S. Kaliskiego 7; 85-796 Bydgoszcz

[l] Łukasiewicz Research Network – PORT Polish Centre for Technology Development, Stablowicka 147, 54-066 Wroclaw, Poland
[m] Istituto di Struttura della Materia (ISM-CNR), Via del Fosso del Cavaliere 100, Rome, 00133, Italy
[n] Dipartimento di Chimica, Biologia e Biotecnologie, Università degli Studi di Perugia & UdR INSTM di Perugia, via Elce di Sotto 8, 06123, Perugia, Italy.
[o] Department of Natural Sciences & Mathematics, College of Sciences & Human Studies, Prince Mohammad Bin Fahd University, Al Khobar 31952, Saudi Arabia.

Keywords: Flexible photovoltaics, perovskite solar cell, interface modification, bulky organic cation, long-term stability

ABSTRACT: Flexible perovskite solar cells triggered a vast interest within the scientific community thanks to their broad commercialization prospects. However, the stability of these devices still poses one of the major concerns on the way to rapid industrial deployment. Here, we demonstrate an effective strategy to improve the technical aspects of this technology, improving the reliability and efficiency values of these devices. We apply large organic ammonium molecules for modifying a buried interface between a hole transporting layer (HTL) and perovskite absorbing material. With the 4-fluorophenethylammonium iodide (FPEAI) we achieve 18.66% efficiency for the large-area (1 cm^2) flexible solar cell, a significant improvement over the pristine device without modification. The applied passivation strategy results in a better hole extraction and reduced non-radiative recombination loss at the buried interface. Moreover, we demonstrate the formation of low dimensional perovskite phases in the vicinity of the hole transporting material upon the incorporation of large ammonium cations. This results in a significantly enhanced thermal, and light-soaking stability of fabricated devices. We obtained no loss in 1000 hours of aging at 85 °C, no loss in 1000 hours of light-soaking at open-circuit, and less than 10% drop in 1000 hours of operation at maximum power point for the optimized passivation treatment with the FPEAI. We

also demonstrate a method for monitoring the structural stability of perovskite thin films upon prolonged illumination, ensued by the amount of molecular iodine being released from the layer.

Introduction

Flexible perovskite solar cells (f-PSCs) garnered a lot of attention in the research community over the last couple of years, thanks to their broad, and tangible commercial prospects.[1] Power conversion efficiency (PCE) reported for the lab-scale f-PSC devices recently exceeded 21%. Attainable high specific powers thanks to the use of lightweight substrates and cost-effective manufacturing methods (roll-to-roll processing) constitute key benefits of this technology.[2] However, detailed performance loss mechanisms and long-term reliability of perovskite devices still require a better understanding and more technical advancements to fully utilize the commercial potential of this technology.

Perovskite thin films, due to their ionic and polycrystalline nature, are characterized by various defects, which derive from interruptions or imperfections in the semiconductor's crystal lattice.[3–5] We can distinguish point defects (vacancies and interstitials) and extended defects (grain boundaries, twining and stacking faults, etc.).[6,7] These defects introduce electronic states within the bandgap, which in turn are responsible for trapping photogenerated charge carriers, an increase of non-radiative recombination rates, and reduced solar cell performance. The majority of recombination losses in perovskite solar cells take place at the interfaces with charge selective layers, primarily due to the higher density of defects within these areas.[8,9] Additionally, these ionic defects can migrate within a perovskite layer in response to external stimuli, such as electric field or light. Iodide defects (vacancies and interstitials) were shown to have the lowest activation energy for charge distribution and are believed to dominate the migration mechanism.[7,10] Such interstitial iodides upon illumination can undergo complex redox reactions, leading to the release

of molecular iodine and the formation of deep trap states (primarily hole traps).[11–13] Defect passivation, especially applied to the surface of perovskite thin films, was widely explored as an effective way to suppress recombination losses and also improve device stability.[14,15] Popular passivation strategies include ionic or coordinating interactions with external materials containing electron-rich (stabilization of positively charged defects) or electron-deficient groups (negatively charged sites). Less attention was paid to the modification of a buried interface. Apart from influencing interfacial electronic effects, the change of surface energy onto which perovskite is grown can alter nucleation and crystallization dynamics, leading to differences in layer morphologies and bulk properties. Recently, Degani *et al.* and Cacovich *et al.* applied large organic ammonium halides to the surface of a hole transporting material (HTM) onto which perovskite films were subsequently formed.[16,17] They primarily observed improved layer uniformities with the elimination of nanovoids at the perovskite/HTM interface. No changes in the material's composition, and dimensionality, or clear passivation effects at the buried interface were observed. Here, we modified a buried interface between HTM and perovskite layer with bulky organic cations (BOC) to improve this electronic contact and perovskite film quality. Additionally, we assessed the influence of fluorination of the organic cation on the effectiveness of this modification approach. By studying lift-off perovskite samples, we show the formation of 2D perovskite phases at the buried interface, revealing the incorporation of large cations into the perovskite lattice. With multiple spectroscopic and electrical characterization techniques, we show improved hole extraction and reduced non-radiative recombination losses at the modified interfaces. Devices with the BOC-modified p-side contact show improved photovoltaic performance (approaching 19% for the champion large-area device on the flexible substrate) and display significantly enhanced long-term reliability in different stability tests (thermal test at 85 °C, operational test at maximum power

point, light soaking test at open-circuit). Moreover, we corroborate these results by identifying the reinforced structural stability of perovskite films upon interface modification, which is evidenced by slower iodine release during continuous light soaking. This is also confirmed by computational modeling of the HTM/perovskite interfaces, with and without modifications.

Results and discussion

Poly(triaryl)amine (PTAA) is one of the most commonly used hole transporting material (HTM) for the p-i-n perovskite solar cells. Its interface with a perovskite thin film can be still a source of performance-limiting, non-radiative recombination losses.[18,19] We applied PTAA surface modification based on large-cation organic halides to improve this electronic contact. We selected phenethylammonium iodide (PEAI) as a modifying compound, which is commonly used for perovskite surface passivation with the ability to form reduced dimensionality perovskite compositions.[20] We also tried a fluorinated variant, 4-fluoro-phenethylammonium iodide (FPEAI), in which cation exhibits a strong molecule dipole moment thanks to the fluorine substitution.[21,22] To evaluate the influence of PTAA modification on photovoltaic properties, we fabricated flexible perovskite solar cells of p-i-n configuration with the following structure: Polyethylene terephthalate (PET)/ indium zinc oxide (IZO)/ (polybis4-phenyl)(2,4,6-trimethylphenyl)amine (PTAA)/ $Cs_{0.17}FA_{0.83}Pb(I_{0.9}Br_{0.1})_3$/ fullerene C_{60}/ bathocuproine (BCP)/ Ag, which we schematically depict in **Figure 1a-b**. Current density – voltage (JV) and stabilized power output (SPO) characteristics of the devices with and without modifications, we show in **Figure 1c-d**. Performance parameters (champion cells and average values of 30 devices) are summarised in **Table 1**. For the pristine device without modification, we recorded an open-circuit voltage (V_{OC}) of 1.05 V, short-circuit current density (J_{SC}) of 22.23 mA/cm^2, fill factor (FF) of 63.99%, and PCE of 16.03%. With the PEAI modification the PCE improved to 18.13% with FF of 74.32%, V_{OC} of

1.08 V, and J_{SC} of 23.32 mA/cm^2. The FPEAI modification yielded enhancements in all the photovoltaic parameters, reaching the best PCE of 18.66% with J_{SC} of 23.34 mA/cm^2, V_{OC} of 1.09 V, and FF of 75.17%. Statistics of all photovoltaic performance parameters, as extracted from the JV characteristics, we show in **Figure S1**. For the representative cells of each variant, we also measured external quantum efficiency (EQE) spectra (see **Figure 1e**) and derived integrated J_{SC} values. JV curves of these cells are shown in **Figure S2**. All the PV parameters for these devices are summarised in **Table S1**. The J_{SC} values derived from the EQE plots were slightly lower than the corresponding currents from the JV curves. Ionic displacement screening an electric field in the perovskite film, which can be more severe during the EQE measurement (longer time at short-circuit conditions), was often suggested as a possible origin for these differences.[23] Nevertheless, the same trend of higher current density values and possibly improved charge extraction (especially in the higher energy region) can be observed in the modified devices.

SAMPLE	PCE BEST (PCE AVERAGE ± SD) [%]	FF BEST (FF AVERAGE ± SD) [%]	V_{OC} BEST (V_{OC} AVERAGE ± SD) [V]	J_{SC} BEST (J_{SC} AVERAGE ± SD) [mA/cm^2]	SPO BEST [%]
PRISTINE	16.03 (14.98 ± 0.85)	63.99 (58.66 ± 2.63)	1.05 (1.04 ± 0.01)	22.23 (21.21 ± 0.55)	14.96

FPEAI	18.66 (17.22 ± 0.78)	75.17 (71.62 ± 3.64)	1.09 (1.07 ± 0.01)	23.34 (22.59 ± 0.50)	17.81
PEAI	18.13 (16.72 ± 0.85)	74.32 (71.17 ± 2.76)	1.08 (1.06 ± 0.01)	23.32 (22.13 ± 0.69)	16.82

Table 1. Photovoltaic parameters extracted from the JV characterization measurements of perovskite solar cells processed with different PTAA surface modifications.

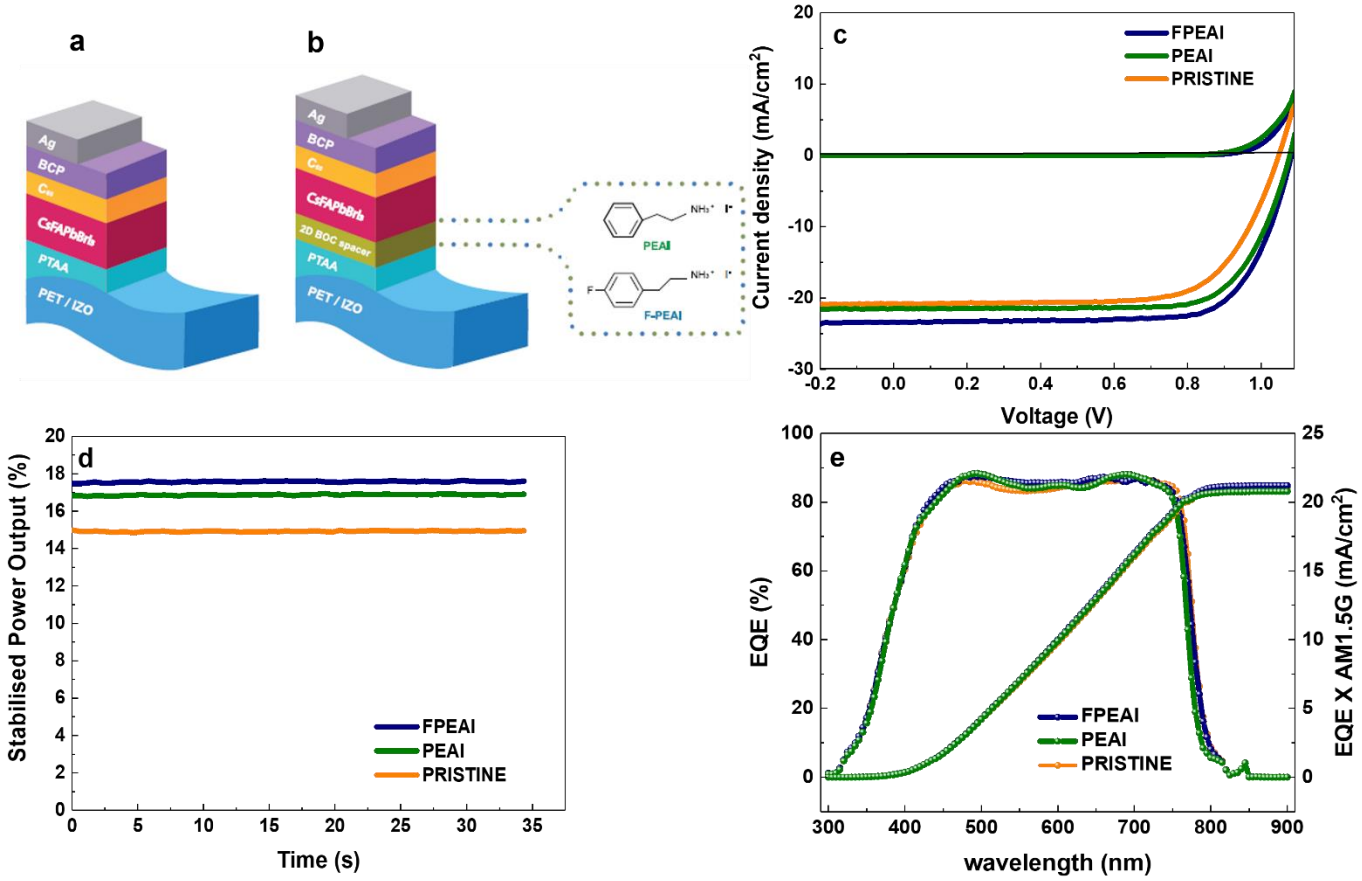

Figure 1. Schematic structures of perovskite solar cells, a) without modification and b) with BOC-based interface modification, c) JV curves of the champion devices of each variation, d) SPO curves for the same devices, e) EQE spectra with integrated current density values of representative devices of each variation.

To study possible interactions of the modifying compounds (PEAI and FPEAI) within the PTAA surface and subsequently forming perovskite material, we performed Density Functional Theory (DFT) simulations. The computational details are presented in **Supplementary Note 1**. Particularly, we evaluated the passivation power of different organic ammonium iodides (FAI – taken as a reference, PEAI, FPEAI) over Pb- and I-terminated $FAPbI_3$ surfaces, which are good approximations of the perovskite material employed in our study (Pb^{2+}, FA^+ and I^- are the main constituents). We depict this mechanism in **Figure 2**. The total passivation energy per spacer molecule, $E_{pass,mol}$, is evaluated by **Equation 1**:

$$E_{pass,mol} = [E_{slab,pass} - (E_{slab,unpass} - 16 * E_{molecule})]/16 \quad (1)$$

where $E_{slab,pass}$ and $E_{slab,unpass}$ are the energies of the passivated and non-passivated slabs, respectively, and $E_{molecule}$ is the energy of the isolated FAI, PEAI, or FPEAI molecule.

The energy is normalized by dividing by the number of the passivating molecules (16), which correspond to the number of the Pb atoms on the two surfaces. For the Pb-terminated surface the $E_{slab,pass}$ energies equal -1.89, -2.22, and -2.26 eV for the FAI, PEAI, and FPEAI, respectively. This highlights how the employed large cations effectively stabilize the perovskite absorber surface through the coordination of the undercoordinated Pb atoms with slightly higher passivation energy found for the FPEAI.

In the case of the I-terminated perovskite surface, we only studied the passivation by PEAI and FPEAI, again obtaining highly spontaneous $E_{pass,mol}$ of -1.64 and -1.66 eV, respectively, which however are lower than values derived for the Pb-terminated surface. Similar observations we found in a previous manuscript.[24] The same conclusions were achieved following a slightly different approach, *i.e.* evaluating the exchange reactions of FA^+/FAI with (F)PEA^+/(F)PEAI up to 3 ions/molecules (**Equation S1-2** and **Figure S3**), showing slightly favored thermodynamics in

the case of FPEAI vs PEAI (see **Table S2**). Overall, this showed that interface modification largely suppressed iodine and lead based point defects. Furthermore, the strong interaction of the FPEAI molecule with the perovskite lattice ($(FPEA)_nFAPbI_3$ structures) could lock in the lead and iodine atoms in their positions, thus mitigating point defect migration within the film. The analysis of the electronic properties, following calculation of the density of states (see **Figure S4**), reveals a significant Fermi energy downshift (~ -0.5 eV) when moving from the PEAI- to the FPEAI-passivated systems. This leads to a different energy alignment between the perovskite valence band and the PTAA hole acceptor level, providing a higher hole injection driving force for the FPEAI system.[25] This could result in higher hole extraction efficacy.

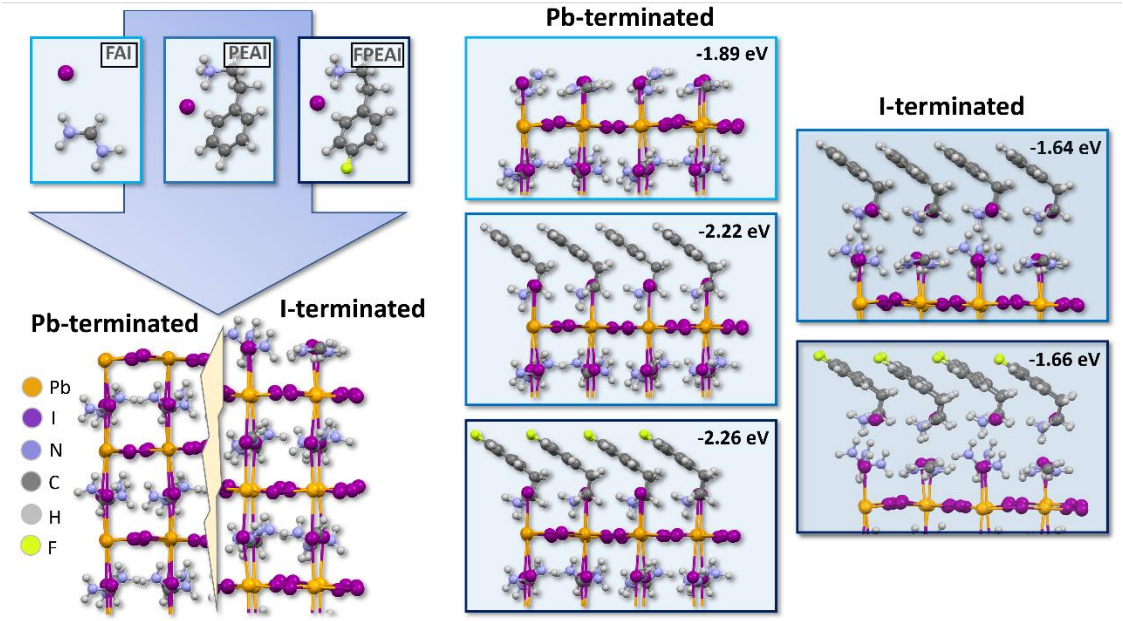

Figure 2. DFT simulation of the passivation of a Pb- and I-terminated perovskite surface. $E_{pass,mol}$ is reported in the inset for each case.

To better understand the influence of a modified surface on the growth of the perovskite layer, we studied the morphology of perovskite films deposited on pristine and modified PTAA films. In **Figure 3a-c**, we show top-view scanning electron microscopy (SEM) images of all the samples.

Cross-section SEM images are shown in **Figure S5**. All three variations show similar microstructures with domain sizes on the level of sub-100 nm. We note that perovskite films on a pristine PTAA show a higher density of nanovoids and pinholes, whereas modified PTAA results in more compact morphologies. This could increase the shunt resistance of the modified devices and contribute to higher FF values. In the cross-section images, we also observe very similar perovskite morphologies for all variations with slightly thicker perovskite films when grown on a FPEAI-modified surface. Additional morphological characterization we carried out with atomic force microscopy (AFM). The surface topography images we show in **Figure S6a-c**. In **Table S3,** we display root mean square (RMS) roughness values for all the studied samples. The layer grown on the FPEAI-modified sample displayed the smoothest surface, possibly due to improved wetting, and more homogenous crystallization. Next, we performed X-ray diffraction (XRD) measurements for all three perovskite sample types. Diffractograms are shown in **Figure 3d**. For the PTAA-modified samples, we observed increased peak intensities at 14.1° and 28.3°, which correspond to (110), and (220) planes of the perovskite structure, respectively. This could originate from enhanced crystallinity or a higher level of grain orientation in these films.[26] Additionally, modified samples, contrary to the pristine PTAA, show no peak at 12.7°, which corresponds to the PbI_2 phase.[27] This implies complete perovskite transformation for these samples. We also applied Williamson-Hall (WH) method to calculate the size of perovskite crystallites and derive microstrain values for the (110), (220) and (330) lattice planes.[28] Obtained results we show in **Table 2** and **Figure S7**. The samples were grown on the FPEAI-modified surface exhibit slightly larger average grain size, and more importantly, reduced microstrain, which can have a significant effect on the layer's optoelectronic quality (defect density, and recombination profile) and ensuing long-term stability.[29] A detailed description of the WH method we provide in **Supplementary**

Note 2. To characterize perovskite crystallographic properties in the vicinity of the PTAA surface, we applied a lift-off process to expose that side of the layer.[30] In short, we thermally evaporated copper layers on top of perovskite films, dipped them in a chlorobenzene solution to dissolve underlying PTAA, and leave free-floating perovskite layers. A more detailed description of the experimental procedure is given in the methods section. Diffractograms of all three perovskite types we show in **Figure 3e**. For the layers grown on surfaces modified with the organic ammonium iodides, we recorded distinct presence of additional peaks at a low angle range (5-6°). We assign these reflections to the (002) lattice plane of the layered (2D) perovskite structure.[31] Similar effect of the 2D/3D heterojunction formation at the buried interface upon application of an appropriate organic ammonium halide was previously reported in literature.[32,33]

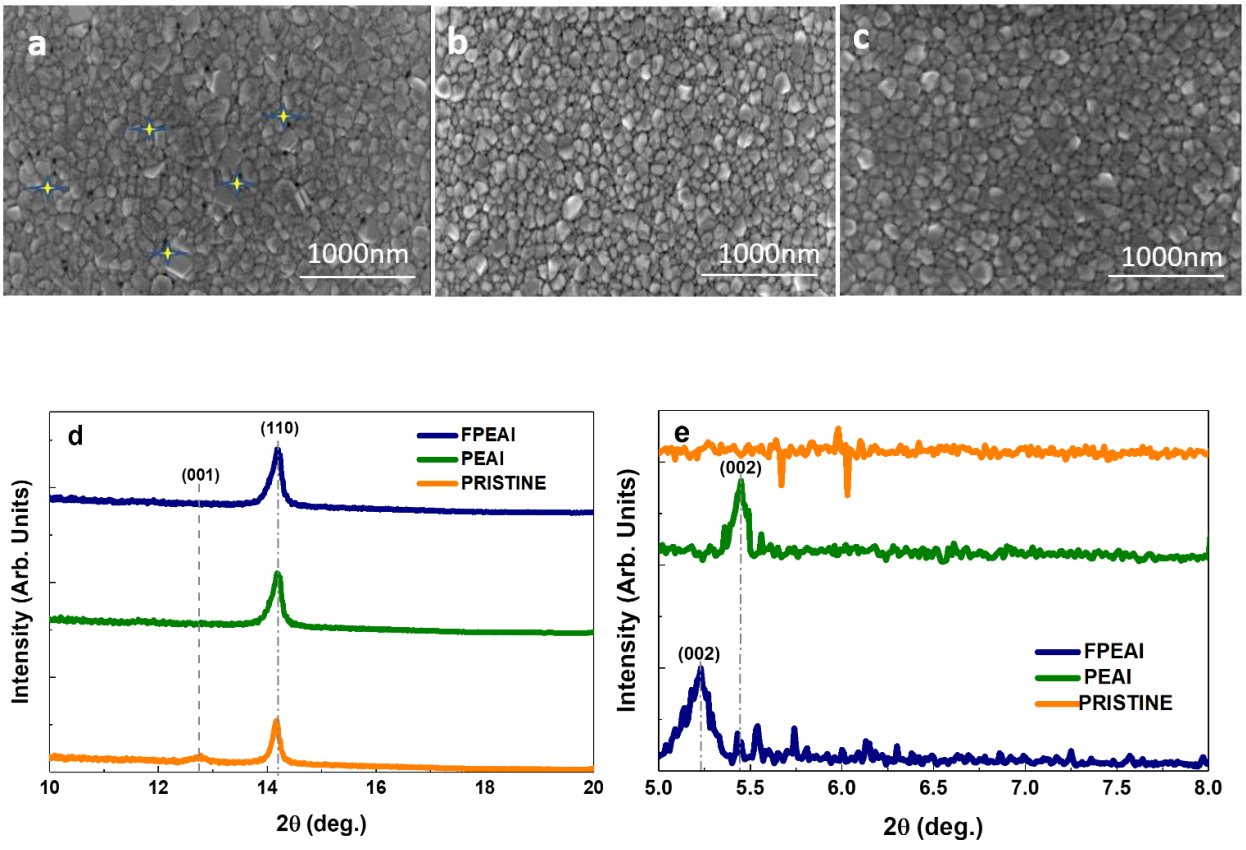

Figure 3. Top-view SEM images of perovskite films, a) without, b) with PEAI- and c) FPEAI-based PTAA modification, appearing nanovoids are marked with yellow stars, d) XRD of

perovskite films of all three variations, e) XRD (zoomed at the low angle part) of the lift-off perovskite films.

Table 2. Average perovskite crystallite sizes, and microstrain values derived from XRD measurements of perovskite thin films processed on PTAA surface with different modifications.

SAMPLE	CRYSTALLITE SIZE [NM]	MICROSTRAIN [%]
FPEAI	59	1.31
PEAI	53	1.57
PRISTINE	49	1.63

Then, we studied the optoelectronic properties of perovskite films grown on modified and unmodified PTAA surface. The samples with interfacial modification display significantly enhanced absorption in the high energy part, below 550 nm (see **Figure S8**), which could originate from the contribution of layered phases.[32] All the films show the same optical bandgap, as derived from the Tauc plot (**Figure S9**). In **Figure 4a**, we show photoluminescence (PL) spectra of the samples with and without interface modification. We note higher PL intensities recorded for the PTAA-modified films, with the FPEAI type showing the highest signal. There was also a noticeable blue-shift (~5 nm) in the PL peak position of the modified samples. The same trends were also observed for the excitation through the other side, in the lift-off perovskite films, see **Figure 4b**. Next, we performed time-resolved PL (TRPL) measurements for the same set of samples. The decay curves (excitation through the perovskite surface and through the lift-off

buried interface) are presented in **Figure 4c-d**. Longer PL lifetimes for the modified samples imply reduced non-radiative loss mechanism (trapping and recombination) in these films. Interestingly, we observed a three-fold increase in lifetime for the interface-modified lift-off samples. This provides strong evidence that PTAA modification with the BOC molecules can effectively reduce non-radiative recombination losses at that interface.[32,33] The PL decays were fitted with a nonlinear exponential function, all the fitting parameters we display in **Table S4**.

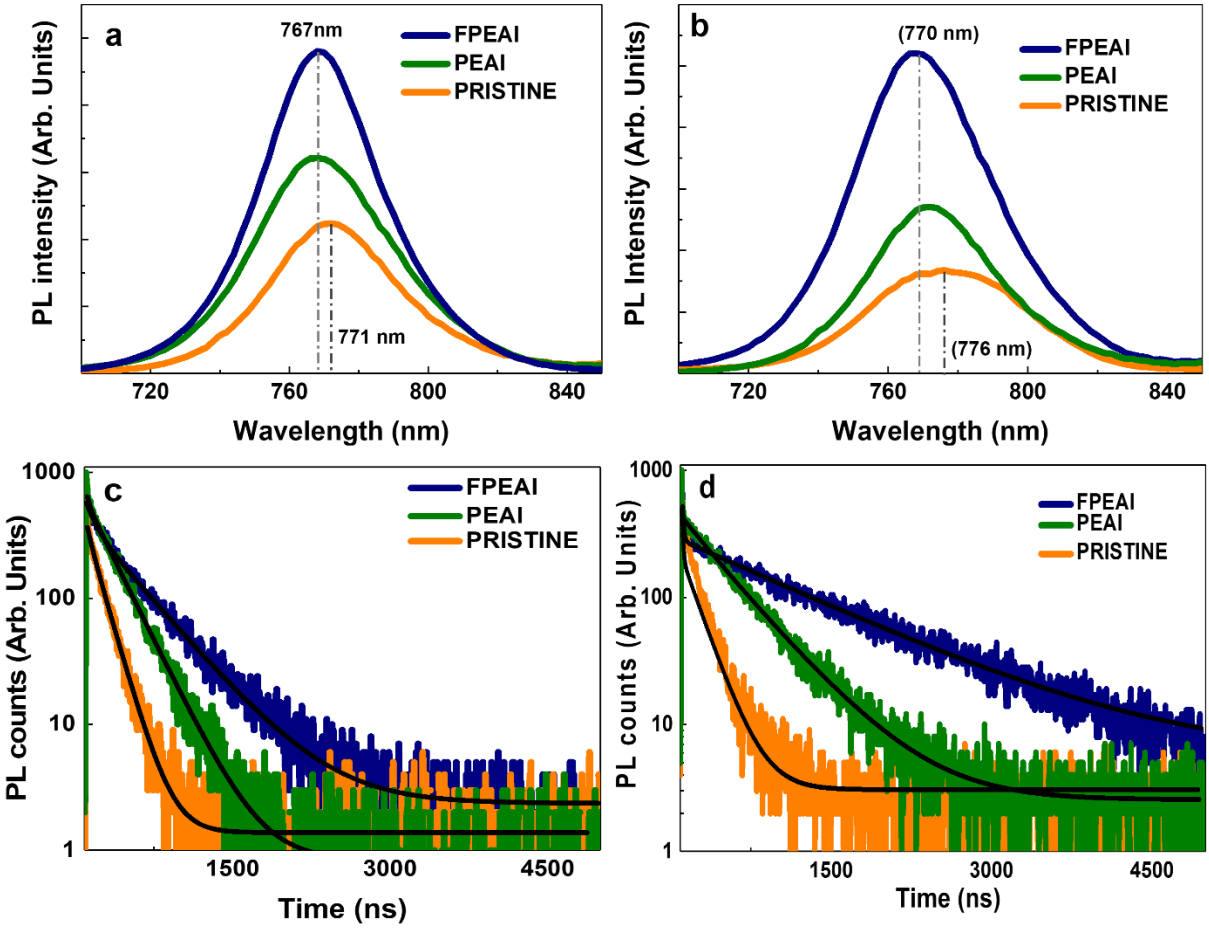

Figure 4. a) Steady-state PL spectra of perovskite films processed on PET/ITO/PTAA substrates, with and without modifications; b) steady-state PL of the same perovskite variations taken for the lift-off samples; c) time-resolved PL decays of the samples from a); d) time-resolved PL decays of the samples from b).

To have a better insight into the charge recombination dynamics in the perovskite layer and at the interfaces, we performed electroluminescence (EL) measurements of complete solar cells. To this end, we applied a forward bias to our devices, with and without PTAA modification, making it operate in a LED mode to study the EL signal. **Figure 5a**, presents the comparison of the EL spectra of the three devices with an applied forward bias of 2 V. The shapes of the EL spectra resemble closely the PL spectra, however the intensity of emission for the FPEAI-modified devices is more than two times higher than the PEAI-modified and pristine devices. In **Figure 5b-c**, we show transient integrated EL intensity and the transient current flowing through the cells with applied 2 V bias. After 20 s of stabilization time, the light emitted from the FPEAI- and PEAI-modified devices has comparable intensities, while emission from the pristine device is about four times lower. The evolution of current values shows similar trends, with the FPEAI- and PEAI-modified cells, displaying around two times higher current than the pristine device. When we confronted recorded light intensities with the current intensities, we noticed that the brightness of the pristine sample is about 3 - 4 times lower than the modified samples, but the current magnitude of the pristine cell is only equal to less than a half of current values measured for the other samples. Therefore, contrary to our previous work, where simple qualitative analysis was sufficient to give indications about devices' efficiencies, in this case, more detailed investigation was necessary.[34] We started with the determination of the devices' V_{OC} radiative limits, following **Equation 2**:[35]

$$V_{OC}^{rad\ limit} = V_{OC} - \frac{kT}{e} ln(EQE_{EL}) \qquad (2)$$

where V_{OC} is open-circuit voltage measured for the cell, k denotes the Boltzmann constant, T is temperature expressed in Kelvins, e stands for the elementary charge and EQE_{EL} is the external quantum efficiency of electroluminescence of the device for the current intensity corresponding to the I_{SC} determined in the photovoltaic measurement. In **Table 3**, we show all the values obtained

for the modified and unmodified samples. The calculated V_{OC} values in the radiative limit increase in the following order: pristine < PEAI < FPEAI, which is in agreement with the trend of measured V_{OC} of these cells. The EQE_{EL} values we show in **Figure S10a-c**. To have more insight into the device operation principles, we also applied the Shockley diode equation to the EL results and determined the ideality factors for these three device variations (see **Supplementary Note 3**).

To further corroborate our findings on the influence of PTAA modification on the recombination characteristics at the perovskite interface, we carried out transient photovoltage (TPV) measurements of complete solar cells. TPV method is performed in a small perturbation regime, where the LED light is illuminating a sample with specific light intensity, and a small overcurrent is sent to the cell, which creates a voltage perturbation on the device in the range of 20 mV. The test is repeated for a range of light intensities. We applied intensities starting from 30.4 up to 160.4 mW/cm^2. In **Figure 5d**, time constants extracted from a single exponential fit of voltage decays at different light intensities were plotted as a function of V_{OC} values, each measured at a given intensity. The FPEAI and PEAI-modified devices displayed higher recombination lifetimes than the control sample. This is in good agreement with the reduced non-radiative recombination loss upon PTAA modification, which was implied by PL and EL analyses.

To investigate the possible influence of the PTAA modification on a hole extraction efficacy, we performed transient photocurrent (TPC) measurements of complete solar cells. TPC is performed in a high perturbation regime. The measuring sample is kept at short circuit and an LED light is illuminating the sample with different intensities. Then, the light is switched off and the current decay is measured and integrated. In **Figure 5e**, we plotted extracted charge as a function of short-circuit current density, measured for a range of light intensities (same as in the TPV measurements). The PTAA-modified devices display improved carrier extraction over the control

sample, with the FPEAI type exhibiting the most effective charge collection (largest integrated charge values). To corroborate these findings, we applied the conductive AFM (c-AFM) technique to measure vertical charge transport properties of perovskite films, when grown on modified and unmodified PTAA layers (sample stack: glass/ITO/PTAA/BOC/perovskite) at different applied biases (-0.5, 0 and 0.5 V). Current maps obtained along the scanned distance (at 0.5 V forward bias) we show in **Figure 5f**. The FPEAI-modified sample showed the highest currents at all different biases. The PEAI-based sample also displayed higher signals than the pristine PTAA. In **Table S5**, we present all the results of c-AFM measurements (dark, light, different biases). This clearly indicates an improved hole transfer at the perovskite/PTAA interface modification, which is in good agreement with the TPC measurements.

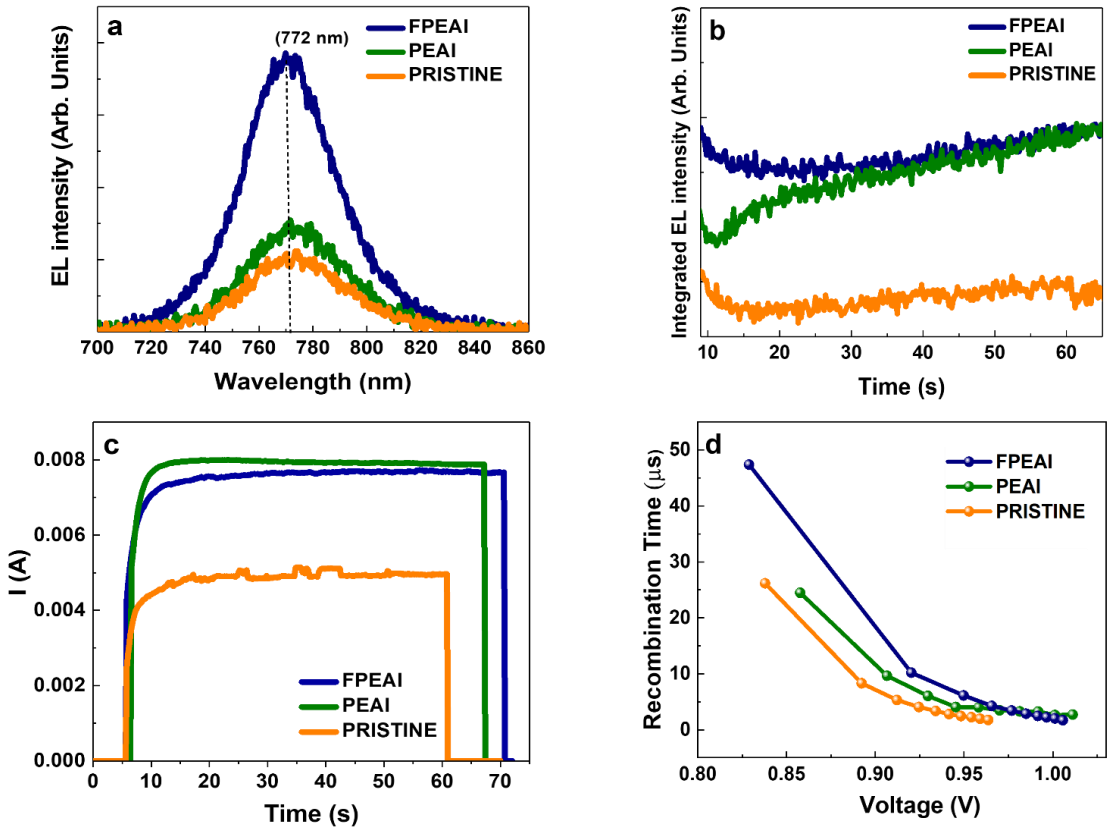

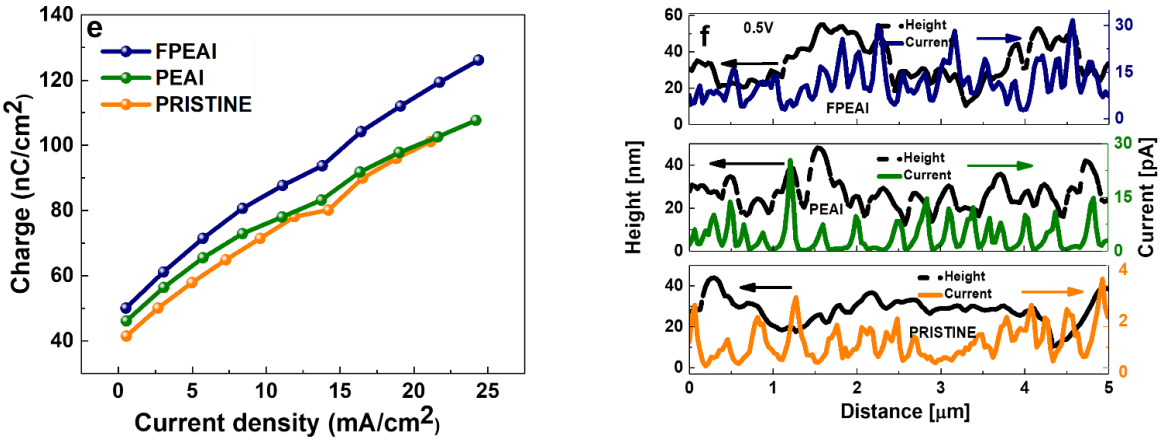

Figure 5. a) EL spectra of the three PSC variations taken at the applied constant bias of 2 V, b) integrated EL intensity of the same cells at 2 V bias, c) current intensities corresponding to the transient EL from the panel b), d) recombination lifetimes of the same cell variations derived from the fitting of photovoltage decays at varied background light intensities, e) charge density extracted from the photocurrent decay measurements taken at varied perturbation light intensities, f) photocurrent values and morphological profile taken across the scanned distance, derived from the c-AFM measurements of perovskite films grown on different surface modifications.

Table 3. Photovoltaic parameters extracted from JV measurements (V_{OC}, I_{SC}), and series of physical parameters derived from electroluminescence measurements (external quantum efficiency of EL, V_{OC} in radiative limit, V_{OC} loss, saturation current, ideality factor 'n' and 'm' are calculated from the current and photon flux respectively).

SAMPLES	V_{OC} (V)	I_{SC} (A)	EQE_{EL}(@I_{SC})	$V_{OC}^{rad\ limit}$ (V)	V_{OC} loss (V)	I_S (A)	n	m
PRISTINE	1.047	0.013	1.06×10^{-4}	1.284	0.23	1.2×10^{-8}	3.8	1.3

PEAI	1.065	0.013	0.92×10^{-4}	1.305	0.24	2.0×10^{-9}	3.0	1.3
FPEAI	1.073	0.014	0.92×10^{-4}	1.314	0.24	7.9×10^{-12}	2.1	1.2

In the next step, we investigated the influence of the PTAA modification strategy on the long-term stability of fabricated perovskite solar cells. For the aging tests, we continued with the double-cation perovskite recipe ($Cs_{0.17}FA_{0.83}Pb(I_{0.9}Br_{0.1})_3$), which is known to provide structurally more stable compositions than the commonly used formulas with the methylammonium cations.[36–38] The reliability analysis we performed following ISOS protocols (International Summit on Organic Photovoltaic Stability), which were recommended for the stability assessment of perovskite PV devices.[39] First, we subjected all the device variations to a thermal stress in dark (85°C, inert atmosphere), compliant with the ISOS-D-2 test. The aging was periodically interrupted for electrical characterization measurements. The evolution of normalized PCE we show in **Figure 6a**. We can observe that the FPEAI-modified devices outperformed the other two types (control and PEAI-modified cells), maintaining nearly 100% of the initial efficiency after 1000 hours of aging. The PEAI-based samples preserved up to 90% of starting PCE, whereas control devices kept only 80% of the initial performance. Corresponding JV curves of the most stable devices of each type (control, FPEAI- and PEAI-modified), which were collected along with the continued aging, we show in **Figure S12**. To understand any structural changes in the perovskite layers upon exposure to elevated temperatures, we also measured XRD of perovskite films (PET/IZO/PTAA/BOC/perovskite), which were subjected to the same heating test (before the test and after 1000 hours of heating). Diffractograms, shown in **Figure S13**, demonstrate improved structural stability of perovskite films, which were grown on the modified PTAA surface. The FPEAI treatment has the strongest stabilization effect and no PbI_2 peak can be observed in this film. For the PEAI modification a small PbI_2 reflection (12.7°) appears after 1000 hours, whereas

for the control sample PbI_2 appears already after 500 hours and significant perovskite degradation is evident at the end of the test.

Next, we studied the effect of light stress on the stability of used perovskite devices (ISOS-L-1 protocol). Solar cells, with and without PTAA modification, were subjected to continuous light soaking (LED source, intensity: ~60 mW/cm^2) in the nitrogen-filled glovebox (inert atmosphere). Devices were aged in two different conditions, at maximum power point (MPP), and open circuit (OC). Electrical characterization measurements were periodically carried out to track the evolution of photovoltaic performance parameters (ca. every 150 hours). In **Figure 6b-c**, we show normalized efficiency values as a function of aging time, extracted from JV scans. The FPEAI-modified devices preserve over 90% and 100% of the initial PCE after 1000 hours of aging at the MPPT, and OC aging conditions, respectively. The PEAI-modified cells were dropping faster in the MPPT test but showed full stability in the OC aging. The control samples were degrading significantly faster in both tests, yielding less than 30%, and around 80% of the initial PCE at the MPPT and OC conditions, respectively. The JV and SPO curves of the best devices, taken along the aging tests (MPPT and OC conditions) for each device variation, are shown in **Figure S14a-i**. All these results clearly show that the cells with the BOC-based PTAA modification exhibit significantly improved long-term reliability upon light exposure. It was previously reported that complex iodide chemistry is one of the major factors affecting the stability of perovskite compositions under illumination.[40,41] Light drives the migration of ionic point defects, such as interstitial iodide ions (I_i) and iodide vacancies (V_i), and triggers photocatalytic chain reactions, leading to oxidation and release of molecular iodine (I_2).[11,42]

To compare the amount of I_2 being released from perovskite films (grown on modified and unmodified PTAA surface) upon prolonged light soaking, we devised a simple experimental setup

based on electrical conductance measurement. A similar approach was reported by Kerner *et al*. to monitor I_2 mass transport through different HTMs.[43] They adopted an electrical Ca corrosion test by replacing Ca with Ag, and took advantage of the susceptibility of Ag to corrosion by I_2. We laminated perovskite samples with glass slides equipped with cavities, where Ag layers were evaporated. Then, by measuring the change in Ag conductance, we were able to relate it to I_2 vapour being released from perovskite films upon light soaking. The schematic of the applied sample structure we show in **Figure S15**. In **Figure 6d** we present normalized conductance values as a function of light soaking time for different perovskite films. The BOC-modified samples show significantly reduced conductance drop, implying slower iodine release, which could be a result of improved structural stability of perovskite films grown on the modified PTAA surfaces. The samples, which were subjected to the light soaking, we additionally characterized by X-ray photoelectron spectroscopy (XPS) to corroborate changes in the chemical composition of the perovskite surface. In **Table 4**, we show extracted I/Pb ratios for different samples, before and after the light soaking test. The spectra for I 3d and Pb 4f are shown in **Figure S16**. The pristine sample shows a decrease in the I/Pb ratio upon light aging, which could imply the release of iodine vapor.[44] Perovskite samples grown on the BOC modified PTAA samples display nearly unchanged I/Pb ratios.

Overall, modification of a buried interface with appropriate large organic cations, which can form low dimensional perovskite phases, provides an effective avenue to reinforce the structural stability of these layers. The reduction of ionic migration effects leads to significantly improved long-term stability of these devices. This can be complementary to perovskite surface modification, where 2D perovskite formation is commonly explored as a strategy for improving stability of these cells.[20]

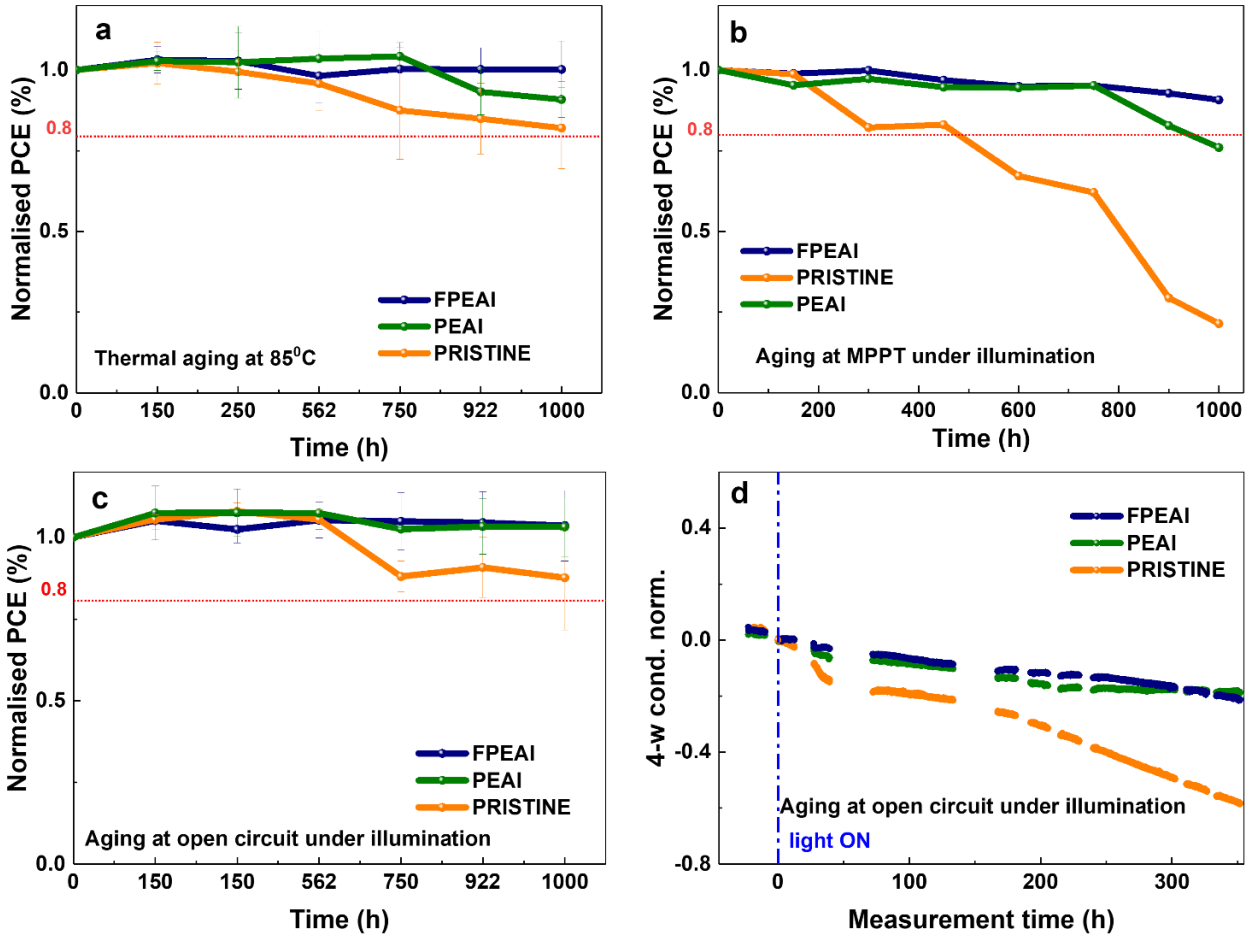

Figure 6. Time evolution of normalised PCE values of the three PSC variations, which were subjected to a) thermal stress test at 85 °C (glovebox), b) continuous operational test at maximum power point (glovebox), c) continuous light soaking test at open-circuit (glovebox), d) time evolution of normalized conductance values of silver films laminated with different perovskite films, measured upon continuous light soaking.

Table 4. Elemental analysis of the surface of three different perovskite variations, before and after 1000 hours of light soaking, derived from XPS measurements.

SAMPLES	%I	%Pb	%O	%C	I/Pb
PRISTINE_0 H	13.73	5.37	9.54	71.25	2.55
PRISTINE_1000 H	11.27	6.86	12.80	69.12	1.64
PEAI_0 H	16.98	6.58	9.89	66.85	2.58
PEAI_1000 H	17.34	6.56	12.56	52.24	2.64
FPEAI_0 H	22.78	8.25	12.95	54.34	2.76
FPEAI_1000 H	23.02	6.93	17.59	56.55	2.85

Conclusions

In this work, we have demonstrated an effective strategy to enhance the performances and stability of flexible perovskite solar cells. By modifying a buried HTM/perovskite interface with bulky organic cations, we not only improve the characteristics of that electronic contact but also reinforce the structural stability of the perovskite material itself. With a range of spectroscopic and electrical characterization techniques, we evidence a reduction in non-radiative recombination loss and improved hole extraction upon PTAA surface modification. This results in over 18% PCE for the large-area flexible PSC, obtained for the FPEAI-based passivation. Crystallographic analysis shows the formation of 2D phases at the buried interface. Notably, all the passivated samples show significantly improved thermal and light soaking stability. The FPEAI modification yields the most effective perovskite reinforcement, with minimal iodine loss and compositional change upon prolonged light soaking. This work paves the way for improving state-of-the-art perovskite solar cell architectures and reaching commercial viability for this technology.

ASSOCIATED CONTENT

Supporting Information. Full description of experimental methods, additional (JV, EQE, EL, TRPL, UV-Vis, FIB-SEM, AFM, XRD, XPS) data and analyses on theoretical modelling and characterization measurements.

AUTHOR INFORMATION

Corresponding Author

*Konrad Wojciechowski - Saule Research Institute; Saule Technologies, Dunska 11, 54-427 Wroclaw, Poland, e-mail: konrad.wojciechowski@sauletech.com

Author Contributions

The manuscript was written through the contributions of all authors. All authors have given approval to the final version of the manuscript.

ACKNOWLEDGMENT

This work was part funded by the Foundation of Polish Science (First TEAM/2017-3/30) and European Union's Horizon 2020 research and innovation program under the grant agreement No 764047 (Espresso project). The authors would like to acknowledge scientific and technical assistance by Saule Technologies Research and Development Team.

REFERENCES

(1) Wojciechowski, K.; Forgács, D.; Rivera, T. Industrial Opportunities and Challenges for Perovskite Photovoltaic Technology. *Sol. RRL* **2019**, *3* (9), 1–9. https://doi.org/10.1002/solr.201900144.

(2) Gao, Y.; Huang, K.; Long, C.; Ding, Y.; Chang, J.; Zhang, D.; Etgar, L.; Liu, M.; Zhang, J.; Yang, J. Flexible Perovskite Solar Cells: From Materials and Device Architectures to Applications. *ACS Energy Lett.* **2022**, *7* (4), 1412–1445. https://doi.org/10.1021/acsenergylett.1c02768.

(3) Siekmann, J.; Ravishankar, S.; Kirchartz, T. Apparent Defect Densities in Halide Perovskite Thin Films and Single Crystals. *ACS Energy Lett.* **2021**, *6* (9), 3244–3251. https://doi.org/10.1021/acsenergylett.1c01449.

(4) Dunfield, S. P.; Bliss, L.; Zhang, F.; Luther, J. M.; Zhu, K.; van Hest, M. F. A. M.; Reese, M. O.; Berry, J. J. From Defects to Degradation: A Mechanistic Understanding of Degradation in Perovskite Solar Cell Devices and Modules. *Adv. Energy Mater.* **2020**, *10* (26), 1–35. https://doi.org/10.1002/aenm.201904054.

(5) Gao, F.; Zhao, Y.; Zhang, X.; You, J. Recent Progresses on Defect Passivation toward Efficient Perovskite Solar Cells. *Adv. Energy Mater.* **2020**, *10* (13). https://doi.org/10.1002/aenm.201902650.

(6) Li, B.; Ferguson, V.; Silva, S. R. P.; Zhang, W. Defect Engineering toward Highly Efficient and Stable Perovskite Solar Cells. *Adv. Mater. Interfaces* **2018**, *5* (22), 1–25. https://doi.org/10.1002/admi.201800326.

(7) Walsh, A.; Stranks, S. D. Taking Control of Ion Transport in Halide Perovskite Solar Cells. *ACS Energy Lett.* **2018**, *3* (8), 1983–1990. https://doi.org/10.1021/acsenergylett.8b00764.

(8) Zhang, S.; Shaw, P. E.; Zhang, G.; Jin, H.; Tai, M.; Lin, H.; Meredith, P.; Burn, P. L.; Neher, D.; Stolterfoht, M. Defect/Interface Recombination Limited Quasi-Fermi Level Splitting and Open-Circuit Voltage in Mono-and Triple-Cation Perovskite Solar Cells. *ACS Appl. Mater. Interfaces* **2020**, *12* (33), 37647–37656. https://doi.org/10.1021/acsami.0c02960.

(9) Xue, J.; Wang, R.; Yang, Y. The Surface of Halide Perovskites from Nano to Bulk. *Nat. Rev. Mater.* **2020**, *5* (11), 809–827. https://doi.org/10.1038/s41578-020-0221-1.

(10) Jiang, F.; Pothoof, J.; Muckel, F.; Giridharagopal, R.; Wang, J.; Ginger, D. S. Scanning Kelvin Probe Microscopy Reveals That Ion Motion Varies with Dimensionality in 2D Halide Perovskites. *ACS Energy Lett.* **2021**, *6* (1), 100–108. https://doi.org/10.1021/acsenergylett.0c02032.

(11) Motti, S. G.; Meggiolaro, D.; Barker, A. J.; Mosconi, E.; Perini, C. A. R.; Ball, J. M.; Gandini, M.; Kim, M.; De Angelis, F.; Petrozza, A. Controlling Competing Photochemical Reactions Stabilizes Perovskite Solar Cells. *Nat. Photonics* **2019**, *13* (8), 532–539. https://doi.org/10.1038/s41566-019-0435-1.

(12) Yang, X.; Ni, Y.; Zhang, Y.; Wang, Y.; Yang, W.; Luo, D.; Tu, Y.; Gong, Q.; Yu, H.; Zhu, R. Multiple-Defect Management for Efficient Perovskite Photovoltaics. *ACS Energy Lett.* **2021**, *6*, 2404–2412. https://doi.org/10.1021/acsenergylett.1c01039.

(13) Ni, Z.; Jiao, H.; Fei, C.; Gu, H.; Xu, S.; Yu, Z.; Yang, G.; Deng, Y.; Jiang, Q.; Liu, Y.; Yan, Y.; Huang, J. Evolution of Defects during the Degradation of Metal Halide Perovskite Solar Cells under Reverse Bias and Illumination. *Nat. Energy* **2022**, *7* (1), 65–73. https://doi.org/10.1038/s41560-021-00949-9.

(14) Li, Y.; Wu, H.; Qi, W.; Zhou, X.; Li, J.; Cheng, J.; Zhao, Y.; Li, Y.; Zhang, X. Passivation of Defects in Perovskite Solar Cell: From a Chemistry Point of View. *Nano Energy* **2020**, *77* (July), 105237. https://doi.org/10.1016/j.nanoen.2020.105237.

(15) Chen, J.; Park, N. G. Materials and Methods for Interface Engineering toward Stable and Efficient Perovskite Solar Cells. *ACS Energy Lett.* **2020**, *5* (8), 2742–2786. https://doi.org/10.1021/acsenergylett.0c01240.

(16) Degani, M.; An, Q.; Albaladejo-Siguan, M.; Hofstetter, Y. J.; Cho, C.; Paulus, F.; Grancini, G.; Vaynzof, Y. 23.7% Efficient Inverted Perovskite Solar Cells by Dual Interfacial Modification. *Sci. Adv.* **2021**, *7* (49), 1–10. https://doi.org/10.1126/sciadv.abj7930.

(17) Cacovich, S.; Vidon, G.; Degani, M.; Legrand, M.; Gouda, L.; Puel, J.-B.; Vaynzof, Y.; Guillemoles, J.-F.; Ory, D.; Grancini, G. Imaging and Quantifying Non-Radiative Losses at 23% Efficient Inverted Perovskite Solar Cells Interfaces. *Nat. Commun.* **2022**, *13* (1), 1–9. https://doi.org/10.1038/s41467-022-30426-0.

(18) Wolff, C. M.; Caprioglio, P.; Stolterfoht, M.; Neher, D. Nonradiative Recombination in Perovskite Solar Cells: The Role of Interfaces. *Adv. Mater.* **2019**, *31* (52). https://doi.org/10.1002/adma.201902762.

(19) Caprioglio, P.; Stolterfoht, M.; Wolff, C. M.; Unold, T.; Rech, B.; Albrecht, S.; Neher, D. On the Relation between the Open-Circuit Voltage and Quasi-Fermi Level Splitting in Efficient Perovskite Solar Cells. *Adv. Energy Mater.* **2019**, *9* (33), 1–10. https://doi.org/10.1002/aenm.201901631.

(20) Wu, G.; Liang, R.; Ge, M.; Sun, G.; Zhang, Y.; Xing, G. Surface Passivation Using 2D Perovskites toward Efficient and Stable Perovskite Solar Cells. *Adv. Mater.* **2022**, *34* (8). https://doi.org/10.1002/adma.202105635.

(21) Qiu, Y.; Liang, J.; Zhang, Z.; Deng, Z.; Xu, H.; He, M.; Wang, J.; Yang, Y.; Kong, L.; Chen, C. C. Tuning the Interfacial Dipole Moment of Spacer Cations for Charge Extraction in Efficient and Ultrastable Perovskite Solar Cells. *J. Phys. Chem. C* **2021**, *125* (2), 1256–1268. https://doi.org/10.1021/acs.jpcc.0c09606.

(22) Shi, J.; Gao, Y.; Gao, X.; Zhang, Y.; Zhang, J.; Jing, X.; Shao, M. Fluorinated Low-Dimensional Ruddlesden–Popper Perovskite Solar Cells with over 17% Power Conversion

Efficiency and Improved Stability. *Adv. Mater.* **2019**, *31* (37), 1–10. https://doi.org/10.1002/adma.201901673.

(23) Mismatch, C. D.; Cells, P. S. Current Density Mismatch in Perovskite Solar Cells. **2020**, 2886–2888. https://doi.org/10.1021/acsenergylett.0c01642.

(24) Yang, B.; Suo, J.; Mosconi, E.; Ricciarelli, D.; Tress, W.; De Angelis, F.; Kim, H. S.; Hagfeldt, A. Outstanding Passivation Effect by a Mixed-Salt Interlayer with Internal Interactions in Perovskite Solar Cells. *ACS Energy Lett.* **2020**, *5* (10), 3159–3167. https://doi.org/10.1021/acsenergylett.0c01664.

(25) Thrithamarassery Gangadharan, D.; Valverde-Chávez, D.; Castro-Méndez, A. F.; Prakash, V.; Izquierdo, R.; Silva, C.; Ma, D.; Correa-Baena, J. P. Bulky Cations Improve Band Alignment and Efficiency in Sn-Pb Halide Perovskite Solar Cells. *ACS Appl. Energy Mater.* **2021**, *4* (3), 2616–2628. https://doi.org/10.1021/acsaem.0c03191.

(26) Yang, J.; Chen, Y.; Tang, W.; Wang, S.; Ma, Q.; Wu, Y.; Yuan, N.; Ding, J.; Zhang, W. H. Crystallization Tailoring of Cesium/Formamidinium Double-Cation Perovskite for Efficient and Highly Stable Solar Cells. *J. Energy Chem.* **2020**, *48*, 217–225. https://doi.org/10.1016/j.jechem.2020.01.012.

(27) Hsiao, K. C.; Jao, M. H.; Li, B. T.; Lin, T. H.; Liao, S. H. C.; Wu, M. C.; Su, W. F. Enhancing Efficiency and Stability of Hot Casting P-i-n Perovskite Solar Cell via Dipolar Ion Passivation. *ACS Appl. Energy Mater.* **2019**, *2* (7), 4821–4832. https://doi.org/10.1021/acsaem.9b00486.

(28) Zhao, Y.; Zhang, J. Microstrain and Grain-Size Analysis from Diffraction Peak Width and Graphical Derivation of High-Pressure Thermomechanics. *J. Appl. Crystallogr.* **2008**, *41* (6), 1095–1108. https://doi.org/10.1107/S0021889808031762.

(29) Jones, T. W.; Osherov, A.; Alsari, M.; Sponseller, M.; Duck, B. C.; Jung, Y. K.; Settens, C.; Niroui, F.; Brenes, R.; Stan, C. V.; Li, Y.; Abdi-Jalebi, M.; Tamura, N.; MacDonald, J. E.; Burghammer, M.; Friend, R. H.; Bulović, V.; Walsh, A.; Wilson, G. J.; Lilliu, S.; Stranks, S. D. Lattice Strain Causes Non-Radiative Losses in Halide Perovskites. *Energy Environ. Sci.* **2019**, *12* (2), 596–606. https://doi.org/10.1039/c8ee02751j.

(30) Yang, X.; Luo, D.; Xiang, Y.; Zhao, L.; Anaya, M.; Shen, Y.; Wu, J.; Yang, W.; Chiang, Y. H.; Tu, Y.; Su, R.; Hu, Q.; Yu, H.; Shao, G.; Huang, W.; Russell, T. P.; Gong, Q.; Stranks, S. D.; Zhang, W.; Zhu, R. Buried Interfaces in Halide Perovskite Photovoltaics. *Adv. Mater.* **2021**, *33* (7), 1–10. https://doi.org/10.1002/adma.202006435.

(31) Sutanto, A. A.; Drigo, N.; Queloz, V. I. E.; Garcia-Benito, I.; Kirmani, A. R.; Richter, L. J.; Schouwink, P. A.; Cho, K. T.; Paek, S.; Nazeeruddin, M. K.; Grancini, G. Dynamical Evolution of the 2D/3D Interface: A Hidden Driver behind Perovskite Solar Cell Instability. *J. Mater. Chem. A* **2020**, *8* (5), 2343–2348. https://doi.org/10.1039/c9ta12489f.

(32) Li, J.; Zuo, L.; Wu, H.; Niu, B.; Shan, S.; Wu, G.; Chen, H. Universal Bottom Contact Modification with Diverse 2D Spacers for High-Performance Inverted Perovskite Solar Cells. *Adv. Funct. Mater.* **2021**, *31* (35), 1–10. https://doi.org/10.1002/adfm.202104036.

(33) Liu, D.; Luo, D.; Iqbal, A. N.; Orr, K. W. P.; Doherty, T. A. S.; Lu, Z. H.; Stranks, S. D.; Zhang, W. Strain Analysis and Engineering in Halide Perovskite Photovoltaics. *Nat. Mater.* **2021**, *20* (10), 1337–1346. https://doi.org/10.1038/s41563-021-01097-x.

(34) Dasgupta, S.; Misztal, K.; Fuentes Pineda, R.; Mróz, W.; Pawlaczyk, Ł.; Serafińczuk, J.; Barker, A. J.; Ahmad, T.; Herman, A. P.; Sahayaraj, S.; Kudrawiec, R.; Petrozza, A.; Dudkowiak, A.; Wojciechowski, K. New Synthetic Route of Ultrapure Alkylammonium Iodides for Perovskite Thin Films of Superior Optoelectronic Properties. *Energy Technol.*

2020, *8* (10), 1–12. https://doi.org/10.1002/ente.202000478.

(35) Rau, U. Reciprocity Relation between Photovoltaic Quantum Efficiency and Electroluminescent Emission of Solar Cells. *Phys. Rev. B - Condens. Matter Mater. Phys.* **2007**, *76* (8), 1–8. https://doi.org/10.1103/PhysRevB.76.085303.

(36) Schwenzer, J. A.; Hellmann, T.; Nejand, B. A.; Hu, H.; Abzieher, T.; Schackmar, F.; Hossain, I. M.; Fassl, P.; Mayer, T.; Jaegermann, W.; Lemmer, U.; Paetzold, U. W. Thermal Stability and Cation Composition of Hybrid Organic-Inorganic Perovskites. *ACS Appl. Mater. Interfaces* **2021**, *13* (13), 15292–15304. https://doi.org/10.1021/acsami.1c01547.

(37) Castriotta, L. A.; Matteocci, F.; Vesce, L.; Cina, L.; Agresti, A.; Pescetelli, S.; Ronconi, A.; Markus, L.; Stylianakis, M. M.; Giacomo, F. Di; Mariani, P.; Stefanelli, M.; Speller, E. M.; Alfano, A.; Paci, B.; Generosi, A.; Fonzo, F. Di; Petrozza, A.; Rellinghaus, B.; Kymakis, E.; Carlo, A. Di. Air-Processed Infrared-Annealed Printed Methylammonium-Free 2 Perovskite Solar Cells and Modules Incorporating Potassium-Doped 3 Graphene Oxide as an Interlayer 1. **2021**. https://doi.org/10.1021/acsami.0c18920.

(38) Ahmad, T.; Dasgupta, S.; Almosni, S.; Dudkowiak, A.; Wojciechowski, K. Encapsulation Protocol for Flexible Perovskite Solar Cells Enabling Stability in Accelerated Aging Tests. *Energy Environ. Mater.* **2022**, 0–2. https://doi.org/10.1002/eem2.12434.

(39) Khenkin, M. V.; Katz, E. A.; Abate, A.; Bardizza, G.; Berry, J. J.; Brabec, C.; Brunetti, F.; Bulović, V.; Burlingame, Q.; Di Carlo, A.; Cheacharoen, R.; Cheng, Y. B.; Colsmann, A.; Cros, S.; Domanski, K.; Dusza, M.; Fell, C. J.; Forrest, S. R.; Galagan, Y.; Di Girolamo, D.; Grätzel, M.; Hagfeldt, A.; von Hauff, E.; Hoppe, H.; Kettle, J.; Köbler, H.; Leite, M. S.; Liu, S. (Frank); Loo, Y. L.; Luther, J. M.; Ma, C. Q.; Madsen, M.; Manceau, M.; Matheron, M.; McGehee, M.; Meitzner, R.; Nazeeruddin, M. K.; Nogueira, A. F.; Odabaşı, Ç.;

Osherov, A.; Park, N. G.; Reese, M. O.; De Rossi, F.; Saliba, M.; Schubert, U. S.; Snaith, H. J.; Stranks, S. D.; Tress, W.; Troshin, P. A.; Turkovic, V.; Veenstra, S.; Visoly-Fisher, I.; Walsh, A.; Watson, T.; Xie, H.; Yıldırım, R.; Zakeeruddin, S. M.; Zhu, K.; Lira-Cantu, M. Consensus Statement for Stability Assessment and Reporting for Perovskite Photovoltaics Based on ISOS Procedures. *Nat. Energy* **2020**, *5* (1), 35–49. https://doi.org/10.1038/s41560-019-0529-5.

(40) Motti, S. G.; Meggiolaro, D.; Martani, S.; Sorrentino, R.; Barker, A. J.; De Angelis, F.; Petrozza, A. Defect Activity in Lead Halide Perovskites. *Adv. Mater.* **2019**, *31* (47), 1–11. https://doi.org/10.1002/adma.201901183.

(41) Meggiolaro, D.; Motti, S. G.; Mosconi, E.; Barker, A. J.; Ball, J.; Andrea Riccardo Perini, C.; Deschler, F.; Petrozza, A.; De Angelis, F. Iodine Chemistry Determines the Defect Tolerance of Lead-Halide Perovskites. *Energy Environ. Sci.* **2018**, *11* (3), 702–713. https://doi.org/10.1039/c8ee00124c.

(42) DeQuilettes, D. W.; Zhang, W.; Burlakov, V. M.; Graham, D. J.; Leijtens, T.; Osherov, A.; Bulović, V.; Snaith, H. J.; Ginger, D. S.; Stranks, S. D. Photo-Induced Halide Redistribution in Organic-Inorganic Perovskite Films. *Nat. Commun.* **2016**, *7* (May). https://doi.org/10.1038/ncomms11683.

(43) Kerner, R. A.; Heo, S.; Roh, K.; MacMillan, K.; Larson, B. W.; Rand, B. P. Organic Hole Transport Material Ionization Potential Dictates Diffusion Kinetics of Iodine Species in Halide Perovskite Devices. *ACS Energy Lett.* **2021**, *6* (2), 501–508. https://doi.org/10.1021/acsenergylett.0c02495.

(44) Tan, S.; Yavuz, I.; Weber, M. H.; Huang, T.; Chen, C. H.; Wang, R.; Wang, H. C.; Ko, J. H.; Nuryyeva, S.; Xue, J.; Zhao, Y.; Wei, K. H.; Lee, J. W.; Yang, Y. Shallow Iodine

Defects Accelerate the Degradation of α-Phase Formamidinium Perovskite. *Joule* **2020**, *4* (11), 2426–2442. https://doi.org/10.1016/j.joule.2020.08.016.

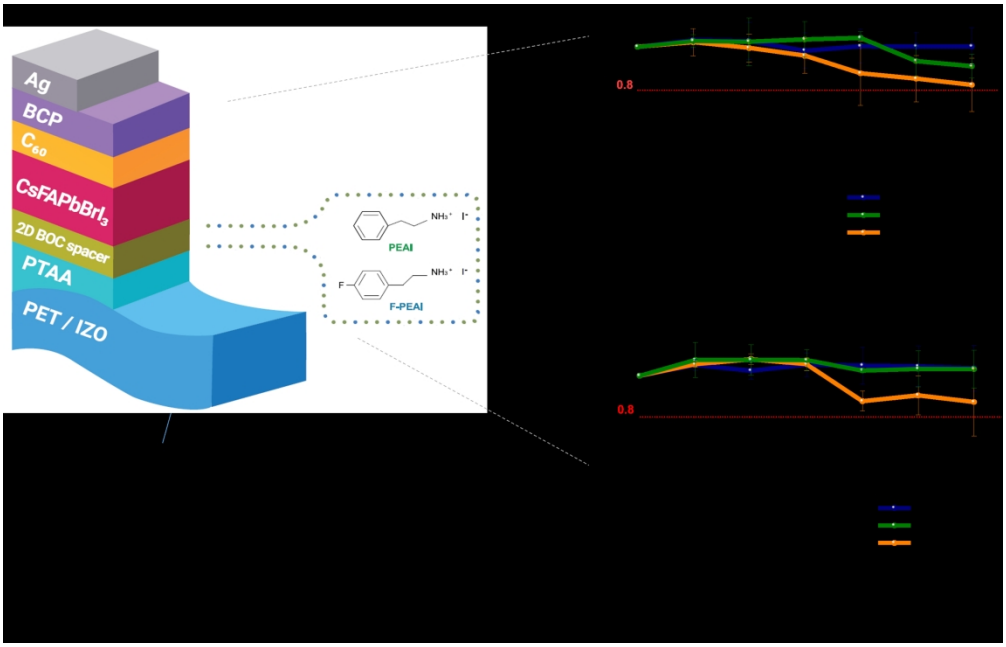

239x152mm (300 x 300 DPI)